Acta Crystallographica Section D
Biological Crystallography
ISSN 0907-4449

Crystal packing in two pH-dependent crystal forms of rhamnogalacturonan acetylesterase

Anne Mølgaard[a,b] and Sine Larsen[a,c]*

[a]Centre for Crystallographic Studies, University of Copenhagen, Universitetsparken 5, DK-2100 Copenhagen, Denmark, [b]Center for Biological Sequence Analysis, Technical University of Denmark, Biocentrum-DTU, Building 208, DK-2800 Lyngby, Denmark, and [c]European Synchrotron Radiation Facility (ESRF), BP 220, F-38043 Grenoble CEDEX, France

Correspondence e-mail: slarsen@esrf.fr

Received 16 September 2003
Accepted 29 December 2003

PDB Reference: rhamnogalacturonan acetylesterase, 1pp4, r1pp4sf.

The glycoprotein rhamnogalacturonan acetylesterase from *Aspergillus aculeatus* has been crystallized in two crystal forms, an orthorhombic and a trigonal crystal form. In the orthorhombic crystal form, the covalently bound carbohydrate at one of the two N-glycosylation sites is involved in crystal contacts. The orthorhombic crystal form was obtained at pH 5.0 and the trigonal crystal form at pH 4.5. In one case, the two crystal forms were found in the same drop at pH 4.7. The differences in crystal packing in the two crystal forms can be explained by the pH-dependent variation in the protonation state of the glutamic acid residues on the protein surface.

1. Introduction

Crystallization of the protein remains as one of the bottlenecks in protein structure determination by X-ray crystallography. The quality of the crystals depends strongly on the intermolecular protein–protein interactions. In a study by Janin & Rodier (1995), protein–protein contacts were analyzed with respect to their number and size, disregarding the chemical nature of the residues engaged in the interactions. They found that the contact areas between protein molecules in crystals are much smaller than those found in biologically active protein complexes, such as an antibody–antigen complex. The areas of the protein buried in crystal contacts are comparable to the interfaces created at random in computer simulations of two proteins tossed against each other (Cherfils *et al.*, 1991). These findings agree with the conclusions reached by Crosio *et al.* (1992) from a study of the protein–protein interactions in six different crystal forms of bovine pancreatic ribonuclease. They found that the interactions were non-specific and involved practically all regions of the protein surface.

Although the crystal packing may generally be non-specific, the literature contains several examples of how the crystallization process can be influenced by selective engineering of the amino-acid residues involved in crystal contacts. Some illustrative examples are the study of glutathione reductase (Mittl *et al.*, 1994) and the cross-linking of a dimer in one of the crystal forms of lysozyme through the formation of disulfide bridges (Heinz & Matthews, 1994). Human H ferritin was genetically modified in the intermolecular-contact region to create a Ca^{2+}-binding site at the site where Cd^{2+} binding took place in the horse and rat enzymes. This chemical change improved the diffraction quality of the crystals significantly (Lawson *et al.*, 1991). In a recent study of aspartyl-tRNA synthetase by Charron *et al.* (2002), point mutations were introduced at the contact surfaces in order to analyse the effect of ionic interactions and hydrophobic contacts. Generally, disruption of contacts, both ionic and hydrophobic,

Table 1
Crystallization.

	Orthorhombic	Orthorhombic and trigonal	Trigonal
Crystallization conditions	1.4 *M* Li_2SO_4 or 1.4 *M* $(NH_4)_2SO_4$, 0.1 *M* NaOAc pH 5.0	19% PEG 4000, 18% 2-propanol, 0.1 *M* citrate buffer pH 4.7	18% PEG 4000, 20% 2-propanol, 0.1 *M* citrate buffer pH 4.5
Space group	$P2_12_12_1$	$P2_12_12_1$ and $P3_121$	$P3_121$
Z	4	4 and 12	12
Unit-cell parameters (Å)			
a	52.14		75.36
b	56.87		
c	71.89		212.30
V_M† (Å^3 Da^{-1})	1.90		3.06
Solvent content (%)	35		60

† Assuming an average glycosylation of 3.5 kDa.

Table 2
Data-collection statistics.

Values in parentheses are for the outer resolution shell.

No. reflections used†	124934
No. rejected‡	5507
Resolution range (Å)	30.0–2.49 (2.62–2.49)
Completeness(%)	98.8 (93.0)
$I/\sigma(I) > 2$ (%)	87.9 (71.6)
R_{merge} (%)	8.7 (45.2)
Multiplicity	5.0 (5.6)
B_{iso} from Wilson plot (Å^2)	56.8

† Number of reflections with a partiality above 0.5. ‡ Number of reflections failing the merging procedure.

hindered crystallization, but when contacts were added the diffraction quality of the crystal was improved.

The pH of the medium may influence the ionic crystal contacts and it is well known that pH can be an important parameter that influences the quality and growth of protein crystals. The variation in the protein charge will be most significant at pH values around the pI of the protein, normally where the solubility is lowest.

Rhamnogalacturonan acetylesterase from *Aspergillus aculeatus* (RGAE) is a 24.6 kDa glycoprotein. Together with rhamnogalacturonan lyases and hydrolases, RGAE degrades the backbone of rhamnogalacturonan I, the highly branched part of pectin, which is one of the major components of the primary cell wall in higher plants (Schols *et al.*, 1990; Kofod *et al.*, 1994; Searle-van Leeuwen *et al.*, 1992; Kauppinen *et al.*, 1995). RGAE is a member of carbohydrate esterase family 12 (Henrissat, 1991) and belongs to the GDS(L) lipase family (Upton & Buckley, 1995), also referred to as the SGNH hydrolase family (Mølgaard *et al.*, 2000). RGAE has been crystallized in orthorhombic and trigonal crystal forms (Mølgaard *et al.*, 1998), both of which were obtained at pH values close to the pI (Kauppinen *et al.*, 1995) of the protein, which makes them suitable for an investigation of crystal packing as a function of pH. The crystal structure of RGAE was determined for the orthorhombic crystal form at 1.55 Å resolution (Mølgaard *et al.*, 2000) and subsequently to a higher resolution (1.12 Å) based on synchrotron-radiation data, which enabled an anisotropic description of the thermal parameters and its carbohydrate structure (Mølgaard & Larsen, 2002). The good diffraction quality of the orthorhombic crystals was unexpected as RGAE is heavily glycosylated. The trigonal crystals are of poorer quality, diffracting to a maximum resolution of 2.5 Å at an in-house source. Both crystal forms appear in the pH range 4.5–5.0, which is close to the pI of RGAE, with the orthorhombic form appearing at the higher pH. Thus, RGAE provides an opportunity to investigate how pH influences crystal packing; we report here the structure determination for the trigonal form of RGAE. In contrast to the orthorhombic form, the trigonal form contains two RGAE molecules in the asymmetric unit. An analysis of the two structures showed that the differences in the crystal packing can be rationalized in terms of the protonation state of the glutamic acid residues on the surface of the protein.

2. Methods

2.1. Crystallization, data collection and processing

The enzyme was crystallized as described previously and two different crystal forms were obtained: an orthorhombic form at pH 5.0 and a trigonal form at pH 4.5 (Mølgaard *et al.*, 1998) (see Table 1). At intermediate pH, both crystal forms were found in the same drop. X-ray intensity data for the trigonal crystal form were collected in-house using a Rigaku R-AXIS IIC image-plate system and were processed using the *HKL* package (Gewirth, 1994) and the *CCP*4 package (Collaborative Computational Project, Number 4, 1994) as previously described (Mølgaard *et al.*, 1998). Experimental details are listed in Table 2.

2.2. Structure determination and refinement

The structure of the trigonal crystal form was solved by molecular replacement (MR) using the previously determined 1.55 Å orthorhombic structure of RGAE (1deo) as a search model. The program used was the original version of *AMoRe* (Navaza, 1994) and reflections in the resolution range 15.0–3.0 Å were used for all MR calculations. The rotation search gave two clear peaks, one for each of the two molecules in the asymmetric unit, with a correlation coefficient of 77.9% and an *R* factor of 27.7%. When the correct space-group symmetry ($P3_121$) was applied to the MR solution, there were no overlaps in the crystal packing.

The structure was refined using *X-PLOR* v.3.851 (Brünger, 1992*b*). The geometry was restrained using the parameter set of Engh & Huber (1991) and 10% of the data were kept out of the refinements and used to calculate an R_{free} value (Brünger, 1992*a*). An initial round of refinement was performed using strict NCS restraints between the two molecules. A bulk-solvent correction was performed using the method of Jiang &

Brünger (1994). No carbohydrate or water molecules were included in this initial model. The electron-density maps were examined and two GlcNAc residues were included in the model, one at each of the two N-glycosylation sites, Asn104 and Asn182. The electron-density maps did not reveal the additional features of the carbohydrate structure that were identified in the orthorhombic form. The next round of refinement was performed using restrained NCS. The initial weights on the NCS restraints were taken as the default values from *X-PLOR* and were applied to all residues. After this, a round of rebuilding was performed and water molecules were added. The residues involved in crystal contacts were identified and the NCS restraints were loosened for these residues. A round of slow-cooling simulated annealing was performed to allow these residues to adopt independent conformations. The final round of refinement yielded R = 0.182 and $R_{\rm free}$ = 0.222. The final model included two molecules, each with 233 amino-acid residues, two GlcNAc residues and 59 water molecules. The average B factors for the two molecules were 43.8 and 44.0 Å^2, respectively. The two NCS-related molecules superimpose with an overall r.m.s.d. of 0.096 Å based on the C$^\alpha$ atoms.

2.3. Analysis of crystal packing

The interfaces of the crystal contacts were identified in the orthorhombic and the trigonal crystal forms of RGAE by manual inspection of the structures using the program *TURBO-FRODO* (Roussel & Cambillau, 1992); the accessible surface areas were calculated using the program *NACCESS* (Hubbard & Thornton, 1993). The *CCP*4 program *CONTACT* was used to obtain a list of the pairwise interactions between intermolecular residues (Collaborative Computational Project, Number 4, 1994).

The area buried in an interface is defined in the following as $B_{\rm int} = (A_1 + A_2) - A_{12}$, where A_1 and A_2 represent the accessible surface area of the independent molecules and A_{12} is the accessible area of the pair. $B_{\rm int}$ thus describes the area buried on both molecules involved in the interface. The accessible surface area corresponds to the area covered by rolling a probe with radius 1.4 Å all over the van der Waals surface of the protein (Lee & Richards, 1971). In Tables 3 and 4, each contact is only represented once and the total buried area of all the contacts represents the total area buried for one molecule. In the case of the trigonal crystal form, the total buried area is for the *AB* pair of NCS-related molecules, except for contact 1, which is the contact between the two independent molecules.

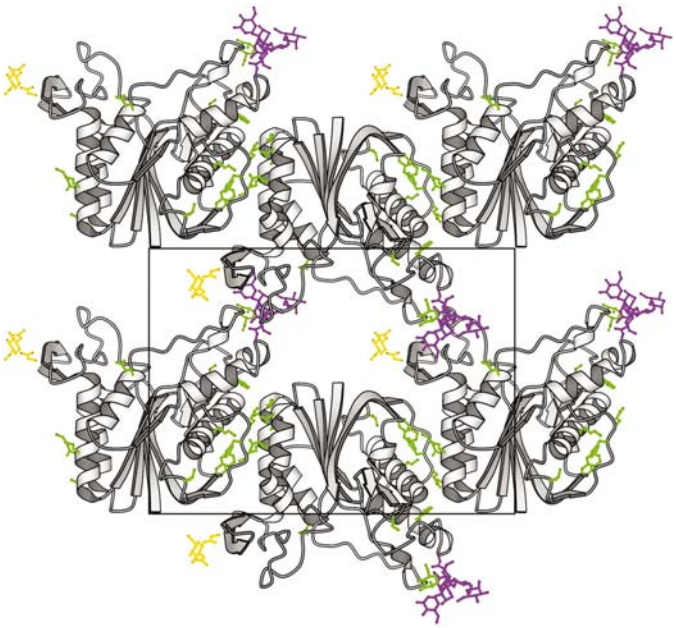

Figure 1
The crystal packing in the *ac* plane in the orthorhombic crystal form, showing the chains of molecules connected by a 2_1 axis along the *c* axis. The carbohydrates at the Asn104 and Asn182 N-glycosylation sites are shown in yellow and purple, respectively. Residues involved in crystal contacts are shown in green. The figure was prepared with the program *MOLSCRIPT* (Kraulis, 1991).

3. Results and discussion

3.1. Overall differences in the crystal packing

When the two molecules from the trigonal crystal form are superimposed with the molecule from the orthorhombic crystal form, the average r.m.s.d. is 0.33 Å based on C$^\alpha$ atoms, indicating that the molecular structure is identical in the two crystal forms. All distances above 0.5 Å correspond to residues involved in different crystal contacts in the two crystal forms, the largest being 1.06 Å for Ser80. The two crystal forms have no crystal contacts in common.

The most obvious difference between the two crystal forms of RGAE is the large difference in packing density. The lower solvent content of ∼35% in the orthorhombic crystal form compared with the ∼60% solvent content in the trigonal crystal form is reflected in the much greater number of crystal contacts in the orthorhombic form (ten per molecule *versus* nine for the *AB* pair of molecules in the trigonal form) and the buried surface area (32% in the orthorhombic crystal form *versus* 17% in the trigonal crystal form) (see Tables 3 and 4). These differences may very well account for the lower diffraction quality of the trigonal crystals of 2.5 Å compared with the 1.55 Å obtained for the orthorhombic crystal form at the in-house source.

Chains of molecules related by crystallographic twofold screw axes are important for the crystal packing in both crystal forms, but the molecules are oriented differently relative to the twofold screw axis in the two crystal forms, leading to distinct differences in the crystal packing. In the orthorhombic crystal form, the chains of molecules generated by the twofold screw axis parallel to *c* (Fig. 1) contains the largest buried area (contact area 1 in Table 3). Together with the contact area between the chains, also shown in Fig. 1 (contact 2 in Table 3), they comprise more than half of the totally buried area per monomer. The interactions of these chains caused by the twofold screw axis parallel to the *b* axis (contacts 3 and 4 in Table 3) form the second strongest interactions. The weakest

Table 3
Crystal contacts in the orthorhombic crystal form.

Contact	Symmetry operation	Total buried area per contact (Å^2)
1	$(-x + 3/2, -y + 1, z - 1/2)$, $(-x + 3/2, -y + 1, z + 1/2)$	1233
2	$(-x + 5/2, -y + 1, z - 1/2)$, $(-x + 5/2, -y + 1, z + 1/2)$	663
3	$(-x + 2, y + 1/2, -z + 3/2)$, $(-x + 2, y - 1/2, -z + 3/2)$	665
4	$(-x + 2, y + 1/2, -z + 1/2)$, $(-x + 2, y - 1/2, -z + 1/2)$	451
5	$(x - 1/2, -y + 1/2, -z + 1)$, $(x + 1/2, -y + 1/2, -z + 1)$	444
Total buried area (Å^2)		3456
Total area in monomer (Å^2)		10790
Fraction of protein surface buried (%)		32

Table 4
Crystal contacts in the trigonal crystal form.

Contact	Symmetry operation	Total buried area per contact (Å^2)
1†	(x, y, z)	1192
2‡	$(-x + 1, -x + y + 1, -z + 1/3)$, $(-x + 1, -x + y, -z + 1/3)$	1059
3	$(-x + 1, -x + y + 1, -z + 1/3)$, $(-x + 1, -x + y, -z + 1/3)$	496
4	$(-x + y, -x + 1, -z - 1/3)$, $(-y + 1, x - y + 1, z + 1/3)$	229
5§	$(y - 1, x, -z)$, $(y, x + 1, -z)$	1053
Total buried area (Å^2)		3433
Total area in molecules $A + B$ (Å^2)		20105
Fraction of protein surface buried (%)		17

† Contact between the two molecules in the asymmetric unit. ‡ *AA* chains. § *BB* chains.

Table 5
Crystal contacts shorter than 3.4 Å in the orthorhombic crystal form.

Contact 1	
Ser29 OG—Lys119*A* NZ	3.33
Ser29 OG—Lys119*B* NZ	3.08
Glu55 OE1—Lys210 NZ	3.12
Glu55 OE1—Phe228 O	3.09
Glu55 OE2—Phe228 O	3.37
Ala58 O—Glu229 OE2A	3.12
Asp59 OD1A—Gly230 N	3.07
Ala123 O—Tyr188 OH	2.76
Lys124 NZ—Glu229 OE2A	3.18
Contact 5	
Ser18 OG—Asp59 O	3.19
Glu55 OE2—Man6 O3	2.71

interactions are along the *a* axis, where there is only one contact area, reflecting the smallest buried area.

The two independent molecules (*A* and *B*) in the asymmetric unit of the trigonal crystal form are not related by point-group symmetry. The interactions between the *A* and *B* molecules comprise the largest buried surface area (contact 1 in Table 4). The *AB* interactions between the two independent molecules in the *AA* and *BB* chains (contact 1) generate layers of molecules in the *ab* plane. The different chains of the *A* and *B* molecules that are generated by the symmetry of the twofold screw axis have a buried area of almost identical size (contacts 2 and 5) that is comparable to the area buried through the interaction between the two independent molecules (contact 1). Figs. 2(*a*) and 2(*b*) illustrate the chains of molecules in the trigonal form and how the interactions between the *AA* and *BB* chains generate layers of molecules in the *ab* plane. The other contacts (3 and 4) lead to smaller buried areas. Contact 3 relates molecules by the threefold screw axis generating the packing with large solvent channels shown in Fig. 2(*c*) formed by alternating *AA* and *BB* layers as shown in Fig. 2(*d*).

The nature of the interactions that form the crystal contacts will be examined more closely in the following in terms of salt bridges, which are known to have an important role in creating intermolecular contacts in crystals and the role of the carbohydrate in crystal packing.

3.2. Analysis of the crystal contacts

Intermolecular contacts of less than 3.4 Å in the two crystal forms are listed in Tables 5 and 6. In the orthorhombic form this only involves contact areas 1 and 5. An unusual feature of the crystal packing in this form is the carbohydrate at the Asn182 N-glycosylation site, which is involved in crystal contacts between four symmetry-related molecules (Mølgaard & Larsen, 2002), as illustrated in Fig. 1. For this reason, the glycan structure at Asn182 is quite well resolved in the electron-density maps in this crystal form. In the trigonal crystal form it is only possible to identify one carbohydrate molecule at each of the two N-glycosylation sites. Table 6 shows that the similar packing of the *AA* and *BB* chains in Figs. 2(*a*) and 2(*b*) is caused by very similar hydrogen-bond interactions between the monomers. Glu202 plays an essential role for the interactions within the *AA* and *BB* chains; its side chain forms hydrogen bonds to the residues in the segment 91–95. One of them is to Glu94; the distances of 2.64 Å (molecule *B*) and 2.81 Å (molecule *A*) are in the range for hydrogen bonds between protonated carboxylic acid groups. Another hydrogen bond that must play a role in the chain formation is the hydrogen bond between the hydroxy group of Ser89 and the backbone carbonyl group of Ser227. A similar short hydrogen bond is seen in the orthorhombic form between the backbone carbonyl of Ala123 and the hydroxy group of Tyr188.

The crystal contacts in the trigonal form do not include any salt bridges; however, the interface between the *A* and *B* molecules contains two very short hydrogen bonds connecting the hydroxy group of Ser*B*18 to the backbone carbonyl of Thr*A*141 and the Ser*A*80 hydroxy to the carboxylate group of Asp*B*59, suggesting that Asp59 is deprotonated. The largest contact in the orthorhombic form involves two salt bridges: Glu55–Lys210 and Lys124–Glu229. The distance between the hydrogen-bond donor and acceptor in the Glu55–Lys210 salt bridge is 3.12 Å and the side chain of Glu229 shows disorder that makes it difficult to define the distance of the hydrogen-bond interactions. Considering the pH of 5 of the crystal-

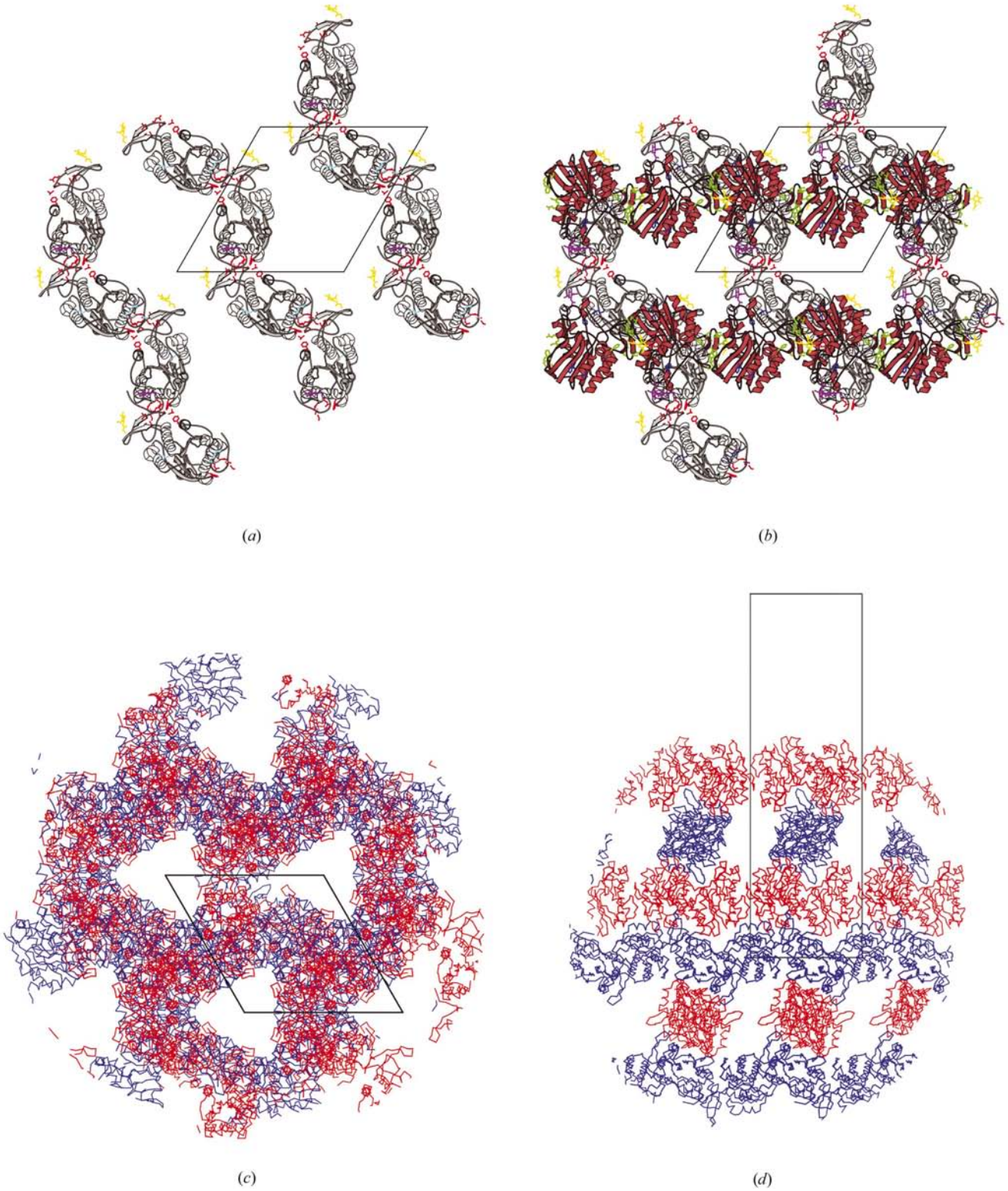

Figure 2
(*a*) The crystal packing in the *ab* plane in the trigonal crystal form, showing only the *AA* chains of molecules connected by a 2_1 axis. The carbohydrates at the Asn104 and Asn182 N-glycosylation sites are shown in yellow and purple, respectively. The residues involved in *AA* crystal contacts are shown in red and those involved in *BB* contacts are coloured green. Interlayer *AB* contacts are shown in blue. (*b*) The same orientation as in Fig. 2(*a*), showing both the *AA* (white) and the *BB* (red) chains. (*c*) Several *AB* layers in the *ab* plane, also shown in Figs. 2(*a*) and 2(*b*). Here, the *AA* chains and *BB* chains are shown in red and blue, respectively. The solvent channels along the *c* axis can be clearly seen. (*d*) The crystal packing in the *ac* plane showing the stacking of the *AA* and the *BB* layers perpendicular to the *c* axis. The *AA* chains and *BB* layers are shown in red and blue, respectively. The figures were prepared with the programs *MOLSCRIPT* (Kraulis, 1991) and *O* (Jones *et al.*, 1991).

lization conditions relative to the pK value for the Glu side chain (4.3–4.5) and the presence of positive charge close to the side chains of Glu55 and Glu229, it is likely that they are negatively charged. In the trigonal crystal form, Glu55 points out into the solvent with no intramolecular contacts shorter than 3.4 Å. Glu229 OE1 accepts a hydrogen bond from the backbone amide of a symmetry-related Val95; OE2 does not participate in any hydrogen bonds.

The molecules in the orthorhombic form contain a very short hydrogen bond (2.49 Å) between Glu202 and Glu206 corresponding to the very strong hydrogen bond observed between carboxylic acid and carboxylate groups, which implies that one of them must be deprotonated. Glu202 accepts an additional hydrogen bond from Tyr30 in the same molecule, but neither of the two glutamic acid residues are directly involved in crystal contacts. Their other hydrogen-bond partners are water molecules. The glutamic acid–water molecule hydrogen bonds are all relatively short, between 2.70 and 2.82 Å.

As mentioned earlier, the same two Glu residues and Glu94 are engaged in the contacts in the *AA* and *BB* chains in the trigonal form (Table 6 and Fig. 2*b*). Glu206 is hydrogen bonded to the backbone carbonyl group of Ser89, showing that the Glu206 side chain must be protonated. The hydrogen-bond pattern around Glu202 is more complex, as shown in Fig. 3. Glu202 OE2 accepts a hydrogen bond from OG1 from a symmetry-related Thr91. Four potential hydrogen-bonding partners are within 3.2 Å of OE1: two backbone amide hydrogen-bond donors and two hydrogen-bond partners which may be donors or acceptors, a water molecule and Glu94 OE2. The protonation state of Glu202 cannot therefore be determined unambiguously from the hydrogen-bonding pattern. However, the hydrogen-bonding distances involving these glutamic acid side chains are generally longer in the trigonal crystal form than in the orthorhombic form, which suggests that they are protonated in the trigonal form. Glu94, another residue that is engaged in the crystal contacts in the trigonal form, is engaged in an intramolecular hydrogen bond in the orthorhombic from to the backbone amide group of Gly92. All other glutamic acids either have identical conformations in the two crystal forms or point out into the solvent.

Of the nine crystal contacts formed for the pair of molecules in the trigonal crystal form (Table 4), four of them are intra-chain *AA* and *BB* contacts, including the three glutamic acids discussed here. These intra-chain contacts represent 62% of the total buried area and thus a small part of the protein surface constitutes the major packing interaction in this crystal form.

Table 6
Crystal contacts shorter than 3.4 Å in the trigonal crystal form.

AA contacts		*BB* contacts	
Contact 2		Contact 5	
Tyr*A*30 OH—Gly*A*90 N	3.36	Tyr*B*30 OH—Gly*B*90 N	3.36
		Ser*B*78 OG—Thr*B*226 OG1	2.92
Leu*A*79 N—Ser*A*227 OG	3.05	Leu*B*79 N—Ser*B*227 OG	2.75
		Ser*B*80 OG—Thr*B*226 OG1	3.21
Ser*A*89 N—Ser*A*227 O	3.37	Ser*B*89 N—Ser*B*227 O	3.36
Ser*A*89 OG—Ser*A*227 O	2.67	Ser*B*89 OG—Ser*B*227 O	2.78
Ser*A*89 O—Glu*A*206 OE2	3.24	Ser*B*89 O—Glu*B*206 OE2	2.94
Gly*A*90 N—Tyr*A*30 OH	3.36	Gly*B*90 N—Tyr*B*30 OH	3.36
Thr*A*91 N—Glu*A*202 OE1	2.98	Thr*B*91 N—Glu*B*202 OE1	3.13
Thr*A*91 N—Glu*A*202 OE2	3.30	Thr*B*91 N—Glu*B*202 OE2	3.38
Thr*A*91 OG1—Glu*A*202 OE1	2.97	Thr*B*91 O—Glu*B*202 OE1	3.15
Thr*A*91 OG1—Glu*A*202 OE2	2.81	Thr*B*91 OG1—Glu*B*202 OE2	2.89
Glu*A*94—OE1 Glu*A*202 OE1	3.40	Glu*B*94 OE1—Glu*B*202 OE1	3.33
Glu*A*94 OE2—Glu*A*202 OE1	2.81	Glu*B*94 OE2—Glu*B*202 OE1	2.64
Val*A*95 N—Glu*A*229 OE1	3.14		
Val*A*95 O—Gly*A*230 N	3.37		
		Phe*B*144 O—Lys*A*124 NZ	3.13
AB contacts			
Contact 1			
Ser*A*9 OG—Asp*B*101 OD2	3.20		
Gly*A*42 N—Asp*B*101 O	3.34		
Asn*A*74 OD1—Asp*B*101 OD1	2.82		
Ser*A*78 OG—Asn*B*56 OD1	2.92		
Ser*A*80 OG—Asp*B*59 OD2	2.53		
Thr*A*141 O—Ser*B*18 OG	2.43		
Asp*A*192 OD2—Tyr*B*100 OH	3.30		
His*A*195 NE2—Asp*B*101 OD2	3.03		
Contact 3			
Lys*A*220 NZ—Asp*B*59 O	2.95		
Ser*A*221 OG—Tyr*B*4 OH	3.13		
Thr*A*226 OG1—Asp*B*59 OD2	2.88		
Contact 4			
Lys*A*124 NZ—Phe*B*144 O	3.13		

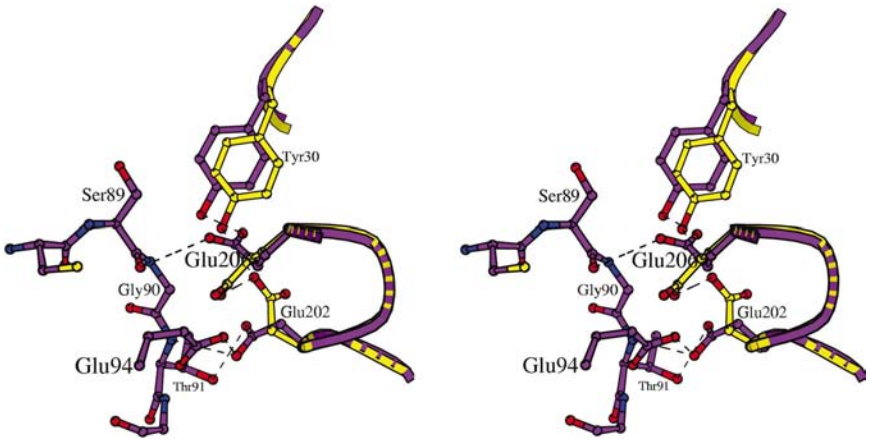

Figure 3
An overlay of the orthorhombic (yellow) and the trigonal (purple) crystal form at the trigonal *AA* and *BB* crystal contacts. The figure was prepared using the program *MOLSCRIPT* (Kraulis, 1991).

The crystal contacts in the orthorhombic crystal form are much less specific and involve a much larger part of the protein surface. The three glutamic acids involved in the major crystal contact in the trigonal crystal form are all engaged in intramolecular hydrogen bonding in the orthorhombic crystal form.

3.3. Discussion

The differences in crystal packing in the two crystal forms of RGAE can be rationalized in terms of the differences in the protonation states of the glutamic acid residues that are located at the patch of the surface which in the trigonal crystal form is involved in the intra-chain *AA* and *BB* crystal contacts: Glu94, Glu202 and Glu206. Small variations in pH close to the pI of the protein influence the overall charge of the protein from neutral in the crystallization conditions for the trigonal form to a more negatively charged protein at pH 5, the crystallization conditions for the orthorhombic form. This change in charge is likely to be accommodated by deprotonation of some of the glutamic acid residues, which have a pK value close to 4.5. Deprotonation of these glutamic acid residues influences the surface charge of the protein and leads to the formation of two salt bridges in the most significant crystal contact area in the orthorhombic crystal form. Also, the main crystal contact in the trigonal crystal form is no longer possible owing to deprotonation of the Glu residues in this area, which leads to the strong intramolecular Glu202–Glu206 hydrogen bond. The significance of the overall charge for the crystallization of RGAE explains why the two crystal forms could be obtained in the same drop at an intermediate pH and shows the significance of pH as a parameter in protein crystallization.

The authors would like to thank Leila Lo Leggio for critical reading of the manuscript. The work was supported by a grant from the Danish National Research Foundation.

References

Brünger, A. T. (1992*a*). *Nature (London)*, **355**, 472–475.
Brünger, A. T. (1992*b*). *X-PLOR Version 3.1. A System for X-ray Crystallography and NMR*. New Haven, CT, USA: Yale University Press.
Charron, C., Kern, D. & Giegé, R. (2002). *Acta Cryst.* D**58**, 1729–1733.
Cherfils, J., Duquerroy, S. & Janin, J. (1991). *Proteins*, **11**, 271–280.
Collaborative Computational Project, Number 4 (1994). *Acta Cryst.* D**50**, 760–763.
Crosio, M. P., Janin, J. & Jullien, M. (1992). *J. Mol. Biol.* **228**, 243–251.
Engh, R. A. & Huber, R. (1991). *Acta Cryst.* A**47**, 392–400.
Gewirth, D. (1994). *The HKL Manual. An Oscillation Data Processing Suite for Macromolecular Crystallography*. New Haven, CT, USA: Yale University Press.
Heinz, D. W. & Matthews, B. W. (1994). *Protein Eng.* **7**, 301–307.
Henrissat, B. (1991). *Biochem. J.* **280**, 309–316.
Hubbard, S. J. & Thornton, J. M. (1993). *NACCESS* computer program. Department of Biochemistry and Molecular Biology, University College London, England.
Janin, J. & Rodier, F. (1995). *Proteins*, **23**, 580–587.
Jiang, J. S. & Brünger, A. T. (1994). *J. Mol. Biol.* **243**, 100–115.
Jones, T. A., Zou, J. Y., Cowan, S. W. & Kjeldgaard, M. (1991). *Acta Cryst.* A**47**, 110–119.
Kauppinen, S., Christgau, S., Kofod, L. V., Halkier, T., Dörreich, K. & Dalbøge, H. (1995). *J. Biol. Chem.* **270**, 27172–27178.
Kofod, L. V., Kauppinen, S., Christgau, S., Andersen, L. N., Heldt-Hansen, H. P., Dörreich, K. & Dalbøge, H. (1994). *J. Biol. Chem.* **269**, 29182–29189.
Kraulis, P. (1991). *J. Appl. Cryst.* **24**, 946–950.
Lawson, D. M., Artymiuk, P. J., Yewdall, S. J., Smith, J. M. A., Livingstone, J. C., Treffy, A., Luzzago, A., Levi, S., Arosio, P., Cesarini, G., Thomas, C. D., Shaw, W. V. & Harrison, P. M. (1991). *Nature (London)*, **349**, 541–544.
Lee, B. & Richards, R. M. (1971). *J. Mol. Biol.* **55**, 379–400.
Mittl, P. R. E., Berry, A., Scrutton, N. S., Perham, R. N. & Schultz, G. E. (1994). *Acta Cryst.* D**50**, 228–231.
Mølgaard, A., Kauppinen, S. & Larsen, S. (2000). *Structure*, **8**, 373–383.
Mølgaard, A. & Larsen, S. (2002). *Acta Cryst.* D**58**, 111–119.
Mølgaard, A., Petersen, J. F. W., Kauppinen, S., Dalbøge, H., Johnsen, A. H., Poulsen, J.-C. N & Larsen, S. (1998). *Acta Cryst.* D**54**, 1026–1029.
Navaza, J. (1994). *Acta Cryst.* A**50**, 157–163.
Roussel, A. & Cambillau, C. (1992). *TURBO-FRODO*. Biographics and AFMB (Architecture et Fonction des Macromolécules Biologiques), Marseille, France.
Schols, H. A., Geraeds, C. C. J. M., Searle-van Leeuwen, M. F., Kormelink, F. J. M. & Voragen, A. G. J. (1990). *Carbohydr. Res.* **206**, 105–115.
Searle-van Leeuwen, M. J. F., van den Broek, L. A. M., Schols, L. A., Beldman, G. & Voragen, A. G. J. (1992). *Appl. Microbiol. Biotechnol.* **38**, 347–349.
Upton, C. & Buckley, J. T. (1995). *Trends Biochem. Sci.* **20**, 178–179.